CHEMISTRY OF MATERIALS

Article

pubs.acs.org/cm

One-Pot Synthesis of In^0 Nanoparticles with Tuned Particle Size and High Oxidation Stability

Christian Kind and Claus Feldmann*

Institut für Anorganische Chemie, Karlsruhe Institute of Technology (KIT), Engesserstraße 15, D-76131 Karlsruhe, Germany.

Supporting Information

ABSTRACT: In^0 nanoparticles with tunable size are obtained via $NaBH_4$-induced reduction of $InCl_3 \cdot 4H_2O$ in diethylene glycol. Citrate-capping allows nucleating almost monodisperse and non-agglomerated In^0 nanoparticles. Effective size tuning is possible in a wide range (10−100 nm) just by varying the concentration of $NaBH_4$, resulting in mean diameters of 8, 55, and 105 nm. The citrate-capped In^0 nanoparticles, moreover, turn out as surprisingly stable against air oxidation. According to XRD and SEM analysis, the 8 nm-sized In^0 particles are molten at room temperature. Size-dependent evolution of the plasmon resonance is observed and results in a brownish-red color and a distinct absorption in the case of the smallest In^0 particles.

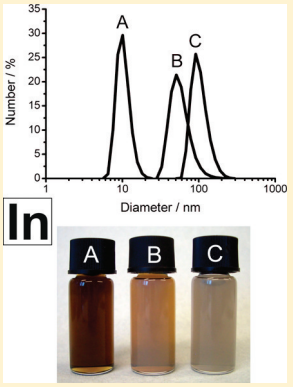

KEYWORDS: *indium, nanomaterial, polyol, citrate, particle size, oxidation stability*

INTRODUCTION

The synthesis of nanoscaled less-noble metals typically is the more elaborate the lower the relevant electrochemical potential. This is related to the high reactivity of less-noble metals, for instance, toward moisture and oxygen. Because of its reactivity, less-noble metals, on the other hand, can be very attractive as a pure element source for a wide range of chemical conversions. Thus, nanoscaled indium ($E_0(In) = -0.34$ V)[1] could serve as a reactive precursor for conversion to, for instance, InN, InP, InAs, In_2O_3, In_2S_3, In_2Se_3, or intermetallic Cu−In phases. As nanomaterials the listed compounds are highly requested for light emitting diodes, transparent conductive oxides, solar cells or heterogeneous catalysis.[2−6] From a more fundamental perspective, In^0 is interesting in view of its quantum-size effects and melting behavior.[7,8]

Nanoscaled In^0 has been yet prepared by gas-phase methods (e.g., laser ablation, evaporation techniques, thermal decomposition of organometallic precursors)[9−12] and advanced liquid-based synthesis (e.g., in polyols, ionic liquids, paraffin) involving complex hydrides, alkali metals, or alkalides/electrides as reducing agents.[13−20] Typically, the synthesis of In^0 involves multistep procedures, phase-transfer reactions, advanced/valuable precursors, special surface cappings and a careful exclusion of moisture and oxygen. In contrast, a facile one-pot synthesis of In^0 that allows to control the particle size and that does neither require advanced precursors nor elaborate inert conditions is presented in the following. Moreover, oxidation stability and size-dependent properties are studied, including the plasmon resonance absorption as well as melting effects.

EXPERIMENTAL SECTION

Synthesis. *General.* The synthesis of the In^0 nanoparticles was performed under dynamic nitrogen purging. All purification and analytic steps were performed under air. All chemicals were applied as received.

In^0 nanoparticles were prepared via a citrate-assisted polyol reaction with diethylene glycol (DEG, Merck, 99%) as the polyol and solvent. First, 2.5 mmol (735 mg) of $InCl_3 \cdot 4H_2O$ (Aldrich, 99.9%) and 1.9 mmol (500 mg) of disodium citrate hydrate (Aldrich, 99%) were filled in a three-necked flask together with 100.0 mL of DEG. Under dynamic nitrogen purging and vigorous stirring, the solution was heated to 100 °C with an oil bath. Subsequently, 25.0 mmol (945.0 mg, In^{3+}:BH_4^- = 1:10, sample A), 7.5 mmol (284 mg, In^{3+}:BH_4^- = 1:3, sample B) and 5.0 mmol (190 mg, In^{3+}:BH_4^- = 1:2, sample C) of $NaBH_4$ (Riedel de Haën, 95%) were dissolved in 2.0 mL of demineralized water and rapidly injected to the transparent, colorless DEG solution. Within seconds, the colorless transparent solutions changed its color to yellow-brown and finally dark brown (sample A), brownish-gray (sample B) and gray (sample C). The nanoparticles were collected by centrifugation of the resulting suspension and were finally washed by sequential redispersion in and centrifugation from ethanol. Colloidally stable dispersions were prepared by resuspending the nanoparticles in ethanol. To obtain powder samples, the nanoparticles were dried at room temperature in air.

Electrostatic Destabilization of 8 nm-Sized In^0 Nanoparticles. Electrostatic destabilization of In^0 nanoparticles was performed by addition of 10.0 mL of a saturated solution of aqueous NaCl to the as-prepared sample A. Subsequent to stirring for 10 min and centrifugation, the solid was washed by redispersion in and

Received: August 2, 2011
Revised: October 8, 2011
Published: October 19, 2011

centrifugation from water and ethanol. The precipitate was redispersed in ethanol and used for further SEM investigation.

Analytical Tools. Scanning electron microscopy (SEM) was conducted on a Zeiss Supra 40VP, using an acceleration voltage of 10−20 kV and a working distance of 2−4 mm. All samples were prepared by evaporation of dispersions in ethanol on a silicon wafer.

Dynamic light scattering (DLS) was performed with a Nanosizer ZS from Malvern Instruments (equipped with a He−Ne laser, detection via noninvasive back scattering at an angle of 173°, 256 detector channels). Suspensions of washed In^0 nanoparticles in ethanol were investigated in polystyrene cuvettes at room temperature.

X-ray powder diffraction (XRD) analysis was carried out with a STOE STADI-P diffractometer using Ge-monochromatized Cu−Kα1 radiation. For the determination of the crystallite size via the Scherrer equation the measured full-width-at-half-maximum (FWHM) was corrected by the contribution of the instrumental broadening. The integral breadth β was calculated by $\beta = (\pi/2)$FWHM.

Fourier-transform infrared spectra (FT-IR) were recorded on a Bruker Vertex 70 FT-IR spectrometer, using KBr pellets. Thus, 400 mg of dried KBr were carefully pestled with 1 mg of the sample and pressed to a thin pellet. The spectra of the nanoparticle samples were subjected to correction of scattering effects to allow for direct comparison to reference spectra.

UV−vis spectra were recorded with a Varian Cary Scan 100. For this purpose, two drops of the as-prepared In^0 suspensions were diluted with 4 mL of diethylene glycol. Measurements were performed in transmission geometry using quartz cuvettes. To allow for direct comparison, the recorded spectra were normalized on the intensity of the citrate absorption at 207 nm. Note that the total concentration of citrate was identical for all the synthesis described above.

■ RESULTS AND DISCUSSION

Synthesis of In^0 and Tuning of the Particle Size. The strategy of synthesis is closely related to the polyol method.[21,22] Concretely, In^0 nanoparticles were prepared applying diethylene glycol (DEG) as the solvent, $InCl_3{\cdot}4H_2O$ as the most common indium source and $NaBH_4$ as the reducing agent. Particle nucleation and growth were controlled, on the one hand, by involving disodium citrate hydrate as colloidal stabilizer and surface capping. On the other hand, hot-injection of aqueous $NaBH_4$ into the solution of $InCl_3{\cdot}4H_2O$ in DEG at 100 °C was applied. The formation of In^0 is indicated by an instantaneous change from a colorless solution to a dark brown suspension. The size of the In^0 nanoparticles is controlled just by varying the amount of $NaBH_4$, ranging from 25.0 mmol (sample A) and 7.5 mmol (sample B) to 5.0 mmol (sample C). In the investigated range, the particle size correlates more or less linearly with the ratio (n) of metal ion (In^{3+}) and reducing agent (BH_4^-) (sample A, n = 0.10; sample B, n = 0.33; sample C, n = 0.50) (cf. Figure S1 in the Supporting Information). In accordance with the model by LaMer and Dinegar on nucleation and growth,[23] the diameter of the In^0 nanoparticles is obviously determined by the number of nuclei formed right at the beginning of the reduction. The success of this measure can be already recognized qualitatively based on the different colors of the resulting suspensions (Figure 1), i.e., dark brown (sample A), brownish-gray (sample B), and gray (sample C).

Size and size distribution of the In^0 nanoparticles were first examined by dynamic light scattering (DLS) (Figure 1). To this concern, the In^0 nanoparticles were carefully washed by sequential centrifugation/redispersion and finally resuspended in ethanol. Via this washing procedure, all remaining starting materials were removed, except for the citrate-capping. DLS analysis evidence a narrow size distribution and a clear difference of the mean hydrodynamic diameters: 10(2) nm (sample A), 58(19) nm (sample B) and 91(27) nm (sample C). In accordance to these data, suspension A is optically transparent, whereas suspensions of samples B and C become more and more opaque (Figure 1).

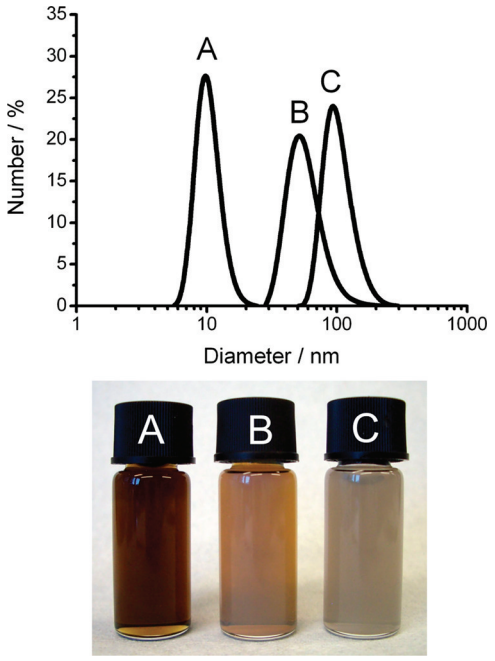

Figure 1. Photos and DLS analysis of citrate-capped In^0 nanoparticles: samples A, B, and C as supensions in ethanol.

Scanning electron microscopy (SEM) confirms the spherical shape as well as the narrow size distribution (Figure 2 and Figure S2 in the Supporting Information). According to a statistical evaluation of at least 500 particles, the In^0 nanoparticles exhibit mean diameters of 8(2) nm (sample A), 55(7) nm (sample B) and 105(10) nm (sample C). Due to the uniform shape, partly dense-packed monolayers were obtained via solvent evaporation on SEM specimens. Although few triangular particles are visible in sample B, the nanoparticles are still very uniform in size (cf. Figure S2 in the Supporting Information). Notably, the particles of sample A become diffuse and deliquescent at high magnification (Figure 3). This finding is accompanied by a loss in contrast on a time scale of 30−60 s and hints to a merging of the 8 nm-sized In^0 under high-energy electron bombardment. Such behavior is well-known, for instance, for Au^0 nanoparticles.[24] A similar behavior can be expected here in view of the low melting point of bulk-In^0 (156 °C).[1] Note that the larger particles of samples B and C do not show any change in shape and structure under the electron beam.

Surface-capping and composition. The excellent colloidal stability of the In^0 nanoparticles is related to the citrate-capping on the particle surface. FT-IR spectra of the In^0 nanoparticles clearly evidence the presence of citrate even after careful washing of the nanoparticles. Although weak in intensity, the characteristic vibrations at 3650−3300 cm^{-1} (ν(OH)), 1650−1250 cm^{-1} (ν(COO) and the fingerprint area (1250−800 cm^{-1}) are well in agreement to citrate reference spectra (Figure 4). In fact, such citrate-capping is well-known to control the colloidal stability of nanoparticles. With gold as the most prominent example,[24,25] citrate-cappings have been used for liquid-phase synthesis of additional metals such as Co, Cu, Ag, Pd, and Pt.[26−29] Less-noble metals such as In^0 with adjustable size in a comparably wide range (i.e., 10−

dx.doi.org/10.1021/cm202256t|Chem. Mater. 2011, 23, 4982−4987

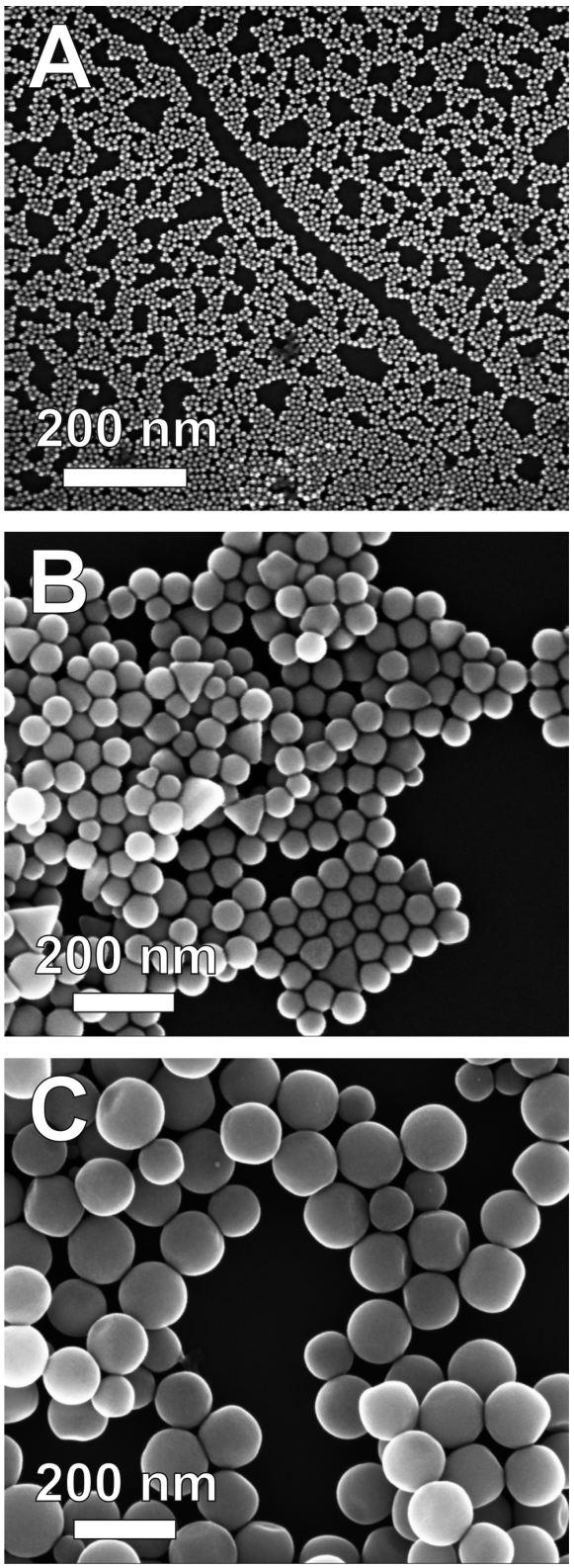

Figure 2. Electron microscopy of citrate-capped In^0 nanoparticles with different diameters: samples A, B, and C.

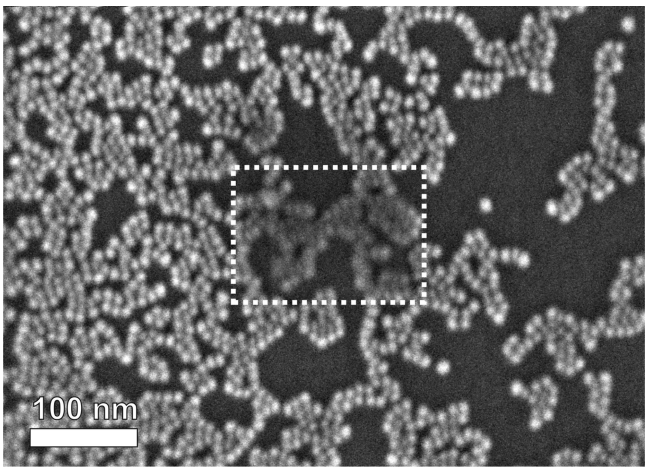

Figure 3. SEM overview image of 8 nm-sized In^0 nanoparticles (sample A) with marked area that has been examined at high magnification (white dashed box).

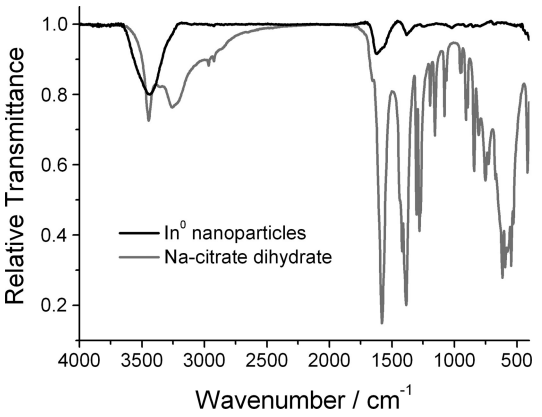

Figure 4. FT-IR spectra indicating the presence of citrate as a surface-capping on In^0 nanoparticles (bulk-sodium citrate shown as a reference).

100 nm) and a high oxidation stability have not yet been described based on citrate as a surface-capping.

Considering the less-noble character of elemental indium (E_0(In) = −0.34 V),[1] fast reoxidation of the nanoparticles would have been expected for suspensions in protic solvents and/or in contact to air. And the In^0 nanoparticles as a powder or dispersed in DEG/ethanol are indeed of limited stability regarding agglomeration and reoxidation if the citrate-capping has been left out. Here, complete decolorization and sedimentation due to reoxidation of In^0 to $In(OH)_3/In_2O_3$ was observed within 12−24 h. In contrast, the citrate-capped In^0 nanoparticles did surprisingly not show any reoxidation − neither as a suspension nor as a powder. This was qualitatively validated by its color (cf. Figure 1) and quantified by X-ray powder diffraction pattern (XRD) (Figure 5). To this concern, the centrifuged and washed samples were dried at room temperature in air. XRD pattern of samples B and C show all characteristic Bragg peaks of elemental indium and indicate the absence of (crystalline) impurities (e.g., $In(OH)_3$, In_2O_3). The most relevant source of error regarding this type of analysis would be the formation of an amorphous oxidation product. Because any oxidation would occur from the outside to the inside of the In^0 nanoparticles, growing of such a noncrystalline oxide shell could be followed upon two effects: (a) the Bragg peaks of the metallic In^0 core would become broader with proceeding oxidation; (b) along with the consumption of In^0, the intensity of Bragg peaks related to In^0 would decrease. A detailed consideration of the most intense Bragg peak of In^0 indicates that both effects do not occur (cf. Figure S3). Even

dx.doi.org/10.1021/cm202256t | Chem. Mater. 2011, 23, 4982–4987

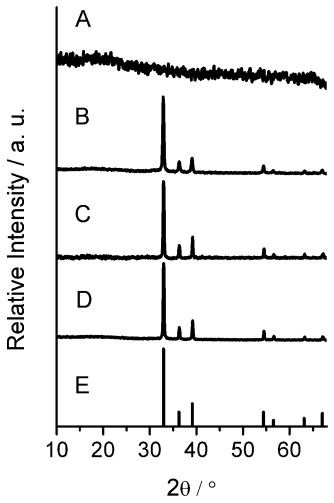

Figure 5. X-ray powder diffraction pattern of citrate-capped In^0 nanoparticles of (A–C) samples A, B, C as well as (D) sample C stored for 8 weeks as a powder in contact to air ((E) bulk-In^0 as a reference, ICDD-No. 3065–929).

when powders of In^0 were left in contact to air for 8 weeks neither any alteration nor any contamination occurred (Figure 5D). On the basis of the integral width of the (101) reflection, a crystallite size of 80–90 nm can be estimated for sample B via the Scherrer equation (including correction of instrumental broadening, cf. Figure S3). This is in reasonable agreement with the values obtained by DLS and SEM. In the case of sample C, such estimation is not meaningful, because broadening of Bragg peaks with particles exceeding diameters of 100 nm is in the range of the instrumental broadening. The fact that the observed Bragg peaks – except for (101) – are low in intensity restricts a determination of the integral peak width. A detailed size–strain separation (e.g., via the Williamson-Hall formalism) would be of limited accuracy and was therefore not performed here.

Room-Temperature Melting and Optical Properties. Surprisingly, X-ray diffraction pattern of sample A did not show any Bragg peak at all (Figure 5A). Considering the crystallinity and purity of samples B and C as well as the stable color of all samples, a complete reoxidation only of sample A to form, for instance, amorphous $In(OH)_3$ can be excluded. If the 8 nm-sized In^0 is however assumed as molten at room temperature, the absence of all Bragg peaks is expected – and again indicates sample A to consist of molten In^0 droplets. In sum, this finding is in accordance to literature data.[8,9,14,16,19] Thus, quantum-mechanical considerations, merging effects under high-energy electron beams and calorimetric studies also point to a melting of indium nanoparticles near room temperature if its diameter is below 10 nm.

The molten state of the 8 nm-sized In^0 particles can be further validated by a simple model and experiment. Thus, the uniform, spherical shape of sample A seems surprising at first glance. Merging of the potentially molten In^0 nanoparticles, on the other hand, might be prevented as long as the electrostatic stabilization of the citrate-capping and the resulting charge repulsion of the nanoparticles remains intact. Taking this model of electrostatically stabilized molten metal droplets for granted, merging of the In^0 nanoparticles should instantaneously occur if the electrostatic stabilization is nullified. As an experiment, this was verified by addition of aqueous NaCl as a strong electrolyte to the as-prepared sample A. In contrast to the well-shaped and well-separated 8 nm-sized In^0 nanoparticles shown in Figure 2, electrostatic destabilization with aqueous NaCl now indeed leads to a merging of the nanoparticles to form droplet-like structures in a size range of 35–60 nm (Figure 6). Note that

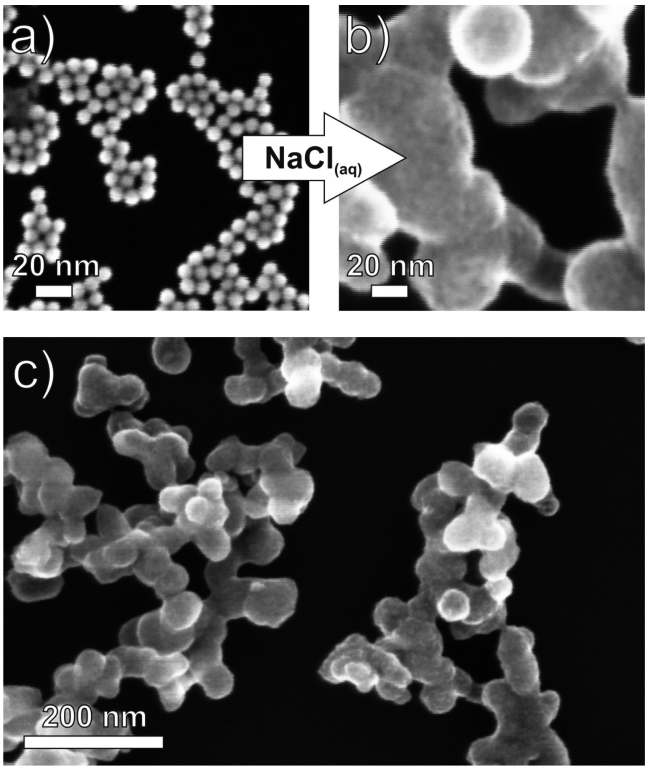

Figure 6. SEM images illustrating the electrostatic destabilization and merging of 8 nm-sized In^0 nanoparticles: detailed images of citrate-capped In^0 nanoparticles (a) after washing with ethanol and (b) subsequent to electrostatic destabilization with NaCl. (c) Typical overview image demonstrating the droplet-like structure of the merged In^0 particles.

such behavior was not observed in the case of the larger particles of sample B and C. Taking all the above findings into account (i.e., behavior under the electron beam, absence of Bragg peaks, merging of particles subsequent to electrostatic destabilization), the molten state of the 8 nm-sized In^0 particles is reliably proven.

Finally, the optical properties of all as-prepared In^0 nanoparticles were quantified via UV–vis spectroscopy (Figure 7). Because of resonant excitation of surface plasmons, the In^0 nanoparticles show strong absorption in the UV range. Position and intensity of the plasmon resonance are well-known as influenced by the particle size and shape as well as by the surface capping and the surrounding solvent.[7,17,30] In recent literature, the surface plasmon resonance (SPR) for In^0 particles, 5–50 nm in diameter, is typically specified to values ranging from 240–290 nm.[16,17,30,31] An evident size-dependent shift of the absorption maximum – as known for Ag^0 or Au^0 nanoparticles – could not be demonstrated for In^0 until now. On the basis of the spherical shape and identical surface-capping and solvent, the presented differently sized In^0 nanoparticles are well-suited for comparing the optical properties and the plasmon resonance. To allow for direct comparison, the recorded spectra were furthermore normalized on the intensity of the citrate absorption at 207 nm. This is

dx.doi.org/10.1021/cm202256t | *Chem. Mater.* 2011, 23, 4982–4987

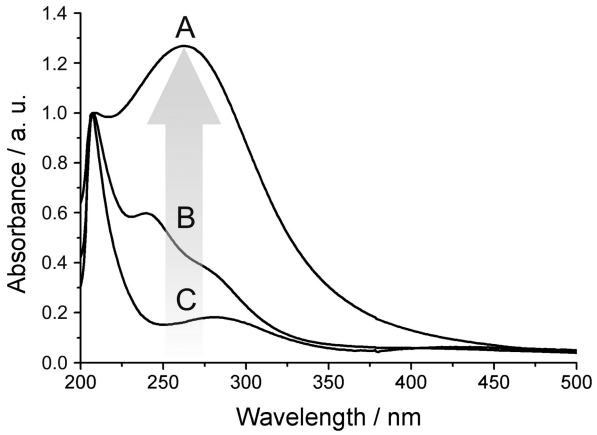

Figure 7. UV−vis spectra of In^0 nanoparticles with different diameters: 8 nm (sample A), 55 nm (sample B), 105 nm (sample C) (all spectra normalized on the intensity of the citrate absorption at 207 nm).

valuable while the total concentration of citrate was identical for all synthesis. A broad and weak absorption at 280 nm is observed for the largest In^0 particles (sample C, 105 nm). For sample B (55 nm) the absorption intensity is increased with maxima at 240 and 280 nm. Such a two-hump structure has been already described for In^0 nanoparticles.[31] The smallest In^0 particles (sample A, 8 nm) exhibit a strong absorption at 264 nm. Altogether, a size-dependent plasmon resonance absorption of the as-prepared In^0 nanoparticles is obvious (Figure 7) and even visible with the naked eye (cf. Figure 1). In contrast to the well-known wavelength-shift as in the case of nanoscale Au or Ag,[24] a distinctive plasmon resonance absorption is here only observed for the smallest In^0 nanoparticles. As a result, the absorption intensity of the as-prepared In^0 is more influenced by the particles size than the wavelength position. This finding is in accordance to other nanoscale metals.[32] The fact that the plasmon-resonance absorption of the smallest 8 nm-sized In^0 is well in accordance with literature data again points to the purity of the nanomaterial. If the surface of In^0 would have been oxidized, the surface plasmon would be very different from a metal surface − and especially the 8 nm-sized In^0 particles can be assumed as most sensitive to air and moisture because of their large specific surface area.

CONCLUSIONS

A facile one-pot synthesis of almost monodisperse In^0 nanoparticles based on common $InCl_3 \cdot 4H_2O$ as a starting material is presented. Just by the amount of the reducing agent $NaBH_4$, the particle size can be adjusted in a wide range, with nanoparticles of 8, 55, and 105 nm in diameter as examples. Citrate is used as a surface capping and guarantees for high colloidal and high oxidation stability of the In^0 nanoparticles. Thus, suspensions and powders can be stored for weeks even in contact to air. This oxidation stability and the absence of oxide impurity phases are validated by powder diffraction analysis and careful consideration of the width and intensity of the Bragg peaks as well as by UV−vis spectroscopy and evaluation of the plasmon-resonance absorption.

Size-dependent properties are observed with regard to melting and color of the In^0 nanoparticles. Thus, the smallest, 8 nm-sized In^0 particles turned out as molten at room temperature. Moreover, distinct plasmon resonance absorption is observed for the 8 nm-sized In^0 particles. The intensity of the plasmon resonance absorption increases significantly when decreasing the particle size and can be visualized even by the naked eye.

ASSOCIATED CONTENT

Supporting Information

Additional figures and information (PDF). This material is available free of charge via the Internet at http://pubs.acs.org.

AUTHOR INFORMATION

Corresponding Author

*Phone: ++49-721-6082855. Fax: ++49-721-6084892. E-mail: claus.feldmann@kit.edu.

ACKNOWLEDGMENTS

The authors are grateful to the German Ministerium für Bildung und Forschung (BMBF) for funding within the project "Nanopartikuläre Dünnschicht-Solarzellen − Grundlagen und Prozesstechnologie (NanoPV)". Here, we explicitly thank Dr. Karen Köhler and Dr. Frank Rauscher (Bayer Technology Services GmbH, Leverkusen) as well as Dr. Erik Ahlswede and Dr. Aina Quintilla (Center for Solar Energy and Hydrogen Research Baden-Württemberg, ZSW) for fruitful collaboration. Finally, we acknowledge the Center for Functional Nanostructures (CFN) of the Deutsche Forschungsgemeinschaft (DFG) at the Karlsruhe Institute of Technology (KIT) for financial support.

REFERENCES

(1) Shriver, D.; Atkins, P. *Inorganic Chemistry*; Oxford Textbooks: London, 2006.
(2) Banin, U.; Millo, O. In Schmid, G., Ed.; *Nanoparticles*; Wiley-VCH: Weinheim, Germany, 2004; pp 305−322, pp 362−367.
(3) Minami, T. *Semicond. Sci. Technol.* **2005**, *20*, S35.
(4) Tang, J.; Hinds, S.; Kelley, S. O.; Sargent, E. H. *Chem. Mater.* **2008**, *20*, 6906.
(5) Li, Y.; Chen, G.; Wang, Q.; Wang, X.; Zhou, A.; Shen, Z. *Adv. Funct. Mater.* **2010**, *20*, 3390.
(6) Takahashi, R.; Yamada, I.; Iwata, A.; Kurahashi, N.; Yoshida, S.; Sato, S. *Appl. Catal., A* **2010**, *383*, 134.
(7) Zhao, Y.; Zhang, Z.; Dang, H. *J. Phys. Chem. B* **2003**, *107*, 7574.
(8) Xie, D.; Wang, M. P.; Qi, W. H.; Cao, L. F. *Mater. Chem. Phys.* **2006**, *96*, 418.
(9) Allen, G. L.; Bayles, R. A.; Gile, W. W.; Jesser, W. A. *Thin Solid Films* **1986**, *144*, 297.
(10) Soulantica, K.; Maisonnat, A.; Fromen, M. C.; Casanova, M. J.; Lecante, P.; Chaudret, B. *Angew. Chem., Int. Ed.* **2001**, *40*, 448.
(11) Henley, S. J.; Carey, J. D.; Silva, S. R. P. *Appl. Surf. Sci.* **2007**, *253*, 8080.
(12) Kar, S.; Santra, S.; Chaudhuri, S. *Cryst. Growth Des.* **2008**, *8*, 344.
(13) Tsai, K. L.; Dye, J. L. *J. Am. Chem. Soc.* **1991**, *113*, 1650.
(14) Zhao, Z.; Zhang, Z.; Dang, H. *J. Phys. Chem. B* **2003**, *107*, 7574.
(15) Jeong, U.; Wang, Y.; Ibisate, M.; Xia, Y. *Adv. Funct. Mater.* **2005**, *15*, 1907.
(16) Singh, P.; Kumar, S.; Katyal, A.; Kalra, R.; Chandra, R. *Mater. Lett.* **2008**, *62*, 4164.
(17) Chou, N. H.; Ke, X.; Schiffer, P.; Schaak, R. E. *J. Am. Chem. Soc.* **2008**, *130*, 8140.
(18) Hammarberg, E.; Feldmann, C. *Chem. Mater.* **2009**, *21*, 771.
(19) Lim, T. H.; Ingham, B.; Kamarudin, K. H.; Etchegoin, P. G.; Tilley, R. D. *Cryst. Growth Design* **2010**, *10*, 3854.
(20) Chen, G.; Wang, L.; Sheng, X.; Yang, D. *J. Sol−Gel Sci. Technol.* **2011**, *58*, 162.
(21) Toneguzzo, P.; Viau, G.; Acher, O.; Guillet, F.; Bruneton, E.; Fievet-Vincent, F.; Fievet, F. *J. Mater. Sci.* **2000**, *35*, 3767.

(22) Feldmann, C.; Jungk, H. O. *Angew. Chem., Int. Ed.* **2001**, *40*, 359.
(23) LaMer, V. K.; Dinegar, R. H. *J. Am. Chem. Soc.* **1950**, *72*, 4847.
(24) Edwards, P. P.; Thomas, J. M. *Angew. Chem., Int. Ed.* **2007**, *46*, 5480.
(25) Turkevich, J.; Stevenson, P. C.; Hillier, J. *Discuss. Faraday Soc.* **1951**, *11*, 55.
(26) Mpourmpakis, G.; Vlachos, D. G. *Phys. Rev. Lett.* **2009**, *102*, 155505.
(27) Park, J. Y.; Lee, H.; Renzas, J. R.; Zhang, Y.; Somorjai, G. A. *Nano Lett.* **2008**, *8*, 2388.
(28) Schwartzberg, A. M.; Olson, T. Y.; Talley, C. E.; Zhang, J. Z. *J. Phys. Chem. B* **2006**, *110*, 19935.
(29) Samim, M.; Kaushik, N. K.; Maitra, A. *Bull. Mater. Sci.* **2007**, *30*, 535.
(30) Khanna, P. K.; Jun, K.-W.; Hong, K. B.; Baeg, J.-O.; Chikate, R. C.; Das, B. K. *Mater. Lett.* **2005**, *59*, 1032.
(31) Cingarapu, S.; Yang, Z.; Sorensen, C. M.; Klabunde, K. J. *Inorg. Chem.* **2011**, *50*, 5000.
(32) Charlé, K.-P.; König, L.; Nepijko, S.; Rabin, I.; Schulze, W. *Cryst. Res. Technol.* **1998**, *33*, 1085.